AIMS Biophysics

http://www.aimspress.com/journal/biophysics

AIMS Biophysics, 4(3): 438-450.
DOI: 10.3934/biophy.2017.3.438
Received: 06 April 2017
Accepted: 18 June 2017
Published: 28 June 2017

Research article

Single cell adhesion strength assessed with variable-angle total internal reflection fluorescence microscopy

Marcelina Cardoso Dos Santos[1,2], Cyrille Vézy[1], Hamid Morjani [3] and Rodolphe Jaffiol[1,*]

[1] Laboratoire de Nanotechnologie et d'Instrumentation Optique, Institut Charles Delaunay, UMR CNRS 6281, Université de Technologie de Troyes, 12 rue Marie Curie, CS 42060, 10 004 Troyes cedex, France

[2] NanoBioPhotonics group, Institute for Integrative Biology of the Cell, Université Paris-Saclay, CNRS, CEA, Bâtiment 430, 91405 Orsay cedex, France

[3] Laboratoire Matrice Extracellulaire et Dynamique Cellulaire, UMR CNRS 7369, Université de Reims Champagne-Ardennes, 51 rue Cognacq-Jay, 51096 Reims Cedex, France

[*] **Correspondence:** rodolphe.jaffiol@utt.fr; Tel: +33-3-25-71-85-27; Fax: +33-3-25-71-84-56.

Abstract: We propose a new strategy to evaluate adhesion strength at the single cell level. This approach involves variable-angle total internal reflection fluorescence microscopy to monitor in real time the topography of cell membranes, i.e. a map of the membrane/substrate separation distance. According to the *Boltzmann* distribution, both potential energy profile and dissociation energy related to the interactions between the cell membrane and the substrate were determined from the membrane topography. We have highlighted on glass substrates coated with poly-L-lysine and fibronectin, that the dissociation energy is a reliable parameter to quantify the adhesion strength of MDA-MB-231 motile cells.

Keywords: biophotonics; total internal reflection fluorescence microscopy; super-resolution microscopy; cell adhesion; cell membrane-substrate interactions

1. Introduction

Cell/microenvironment interactions play an important role in fundamental cellular processes such as proliferation, migration and mechanotransduction. The early stage of these interactions takes place in focal adhesion contacts and involves plasma membrane receptors, such as well known integrins which recognize various ligands located in extracellular environment [1, 2, 3]. In addition to this widely studied specific binding, cells can also interact with their microenvironment through a broad range of nonspecific interactions, resulting from van der Waals forces, electrostatic forces, polymer

steric repulsive forces, or undulation *Helfrich* force [4]. These nonspecific forces can be analyzed by measuring distances from the substrate to the plasma membrane, as forces governing nonspecific interactions are distance-dependent. Several recent publications have shown that specific and nonspecific forces implicated in cellular adhesion (and related processes) appear to have a cooperative action, as regarding the impact of glycocalyx on integrin-mediated adhesion and signaling. The presence of glycocalyx at the cell surface is known for a very long time, but its impact on cell adhesion is still poorly known, although several investigations on biomimetic systems suggest that glycocalyx can exert a nonspecific steric repulsive force [5, 6]. Furthermore, in tumor cells glycocalyx is presumed to mechanically enhance integrin spatial organization and function [7].

In this framework, a lot of different approaches have been proposed to explore cell/microenvironment interactions. Numerous recent techniques allow to measure cell-generated forces, for example by using PDMS micropillar arrays [8] or elastic polymer substrates doped with fluorescent nanobeads [9]. Shear force can also be applied to analyse cell adhesion with microfluidic devices [10] or with fluid microjets [11]. Local measurements on plasma membrane proteins can be achieved by atomic force microscopy (AFM) [12], or with a magnetic tweezers apparatus [1]. Optical microscopy is also widely used to observe specific adhesion such as standard total internal reflection fluorescence (TIRF) microscopy [13] and more spatially-resolved technique such as interferometric photoactivated localization microscopy (iPALM) [14]. The purpose of this paper is not to give an exhaustive overview of all the techniques currently employed to explore cellular adhesion. However, it should be noted that this broad diversity of experimental methods is beneficial to cell biology in order to decipher complex processes such as mechanotransduction.

We present in this paper a new way to quantify the adhesion strength of single cells. This method is based on variable-angle total internal reflection fluorescence microscopy (vaTIRFM). vaTIRFM is an old technique introduced in the mid-80s and quickly forgotten due to the high complexity of the first experimental setup. We have recently proposed an improved straightforward version of vaTIRF adapted to modern TIRF setup [15]. This technique involves the recording of a stack of several TIRF images, by gradually increasing the incident angle of the light beam on the sample. The typical acquisition rate of the stack is about one second. A simple image processing can then be used to restore the cell topography [15], i.e. a map of the distance z_0 between the stained membrane and the substrate, as illustated in Figure 1. The axial resolution of vaTIRFM is very good, typically 10–20 nm, similar to other optical methods that also provide a nanoscale z-resolution, such as reflection interference contrast microscopy (RICM) [16], scanning angle interference microscopy [17], metal-induced energy transfer (MIET) microscopy [18], iPALM [14], or other single-molecule localization super-resolution technique such as dSTORM (direct stochastic optical reconstruction microscopy) combined with supercritical-angle analysis [19].

Compared to other imaging techniques, vaTIRFM presents several advantages (listed in detail in reference [15]). Briefly, cell morphology can be easily examine with conventional bright-field imaging technique such as phase contrast or differential interference contrast, because cells are simply placed on usual glass coverslips. Next, vaTIRFM is not based on single molecule detection. Therefore, it enables observation at the sampling rate of $\approx$1 s together with a very low laser irradiance, typically 10-20 W/cm^2. The surface density of energy is then $\approx$10–20 J/cm^2, that is remarkably smaller than usual dose used in super-resolution techniques: 10^2–10^3 kJ/cm^2 in PALM or STORM and at least 10^4 kJ/cm^2 in stimulated emission depletion (STED) microscopy. Considering

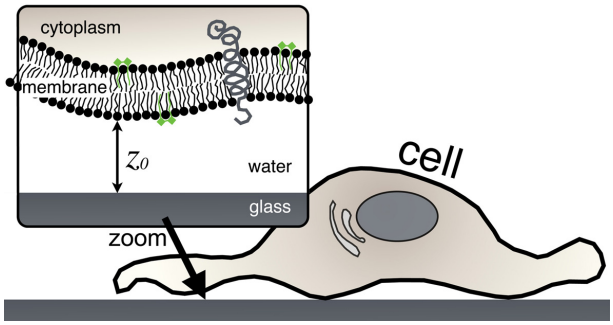

Figure 1. Schematic drawing of a cell spread on a glass substrate. Inset: the plasma membrane is labeled with DiO (in green). z_0 is the distance from the substrate to the plasma membrane.

that the lethal dose of irradiation in fluorescence microscopy is typically few hundreds kJ/cm^2 [20], the high irradiation dose used in most of superresolution imaging techniques (PALM, STORM, STED...) conduct to an important photodamage of the cells, which is not the case in vaTIRFM. Furthermore, to get the cell topography, a simple plasma membrane labeling with common amphiphilic dye is needed. No special protein labeling is required in our experiments. Consequently the cells do not need to be fixed, and they can freely migrate and proliferate on the substrate, which is crucial to observe the dynamic of adhesion process, as intended in this article.

The method introduced in this paper consists in exploiting the time-evolution of the membrane/substrate distance distributions recorded at the single cell level. These distributions are obtained through vaTIRFM measurements, according to the experimental procedure described in a previous publication [15]. From these distance distributions, one can determine the interaction potential between the cell membrane and the substrate, and in a second step a dissociation energy directly related to the adhesion strength. To highlight the strong benefit of this method, we have compared the dynamics of adhesion of MDA-MB-231 motile cells on two different surfaces. The first one is glass coverslip coated with poly-L-lysine. This polymer is well-known to give rise to nonspecific adhesion through electrostatic interactions. On the opposite, to promote specific adhesion, the second surface is glass coverslips coated with a thin layer of fibronectin. Fibronectin is the most used extracellular matrix components in cell adhesion investigations, because cells easily develop binding with fibronectin through many different integrins ($\alpha_3\beta_1$, $\alpha_5\beta_1$, $\alpha_8\beta_1$, $\alpha_v\beta_1$, $\alpha_v\beta_3$) [21]. We recall that MDA-MB-231 cells exhibit on their surface $\alpha_5\beta_1$ and $\alpha_v\beta_1$ integrins [22, 23, 24].

2. Materials and Methods

2.1. Microscope

We propose an improved and straightforward setup for TIRF microscopy well adapted to modern TIRF setup [15]. Our setup allows to tune very precisely the incident angle θ on the sample without any distorsion and important lateral displacement of the illumination zone when the incident angle is increased to reach the evanescent regime. Interestingly, no azimuthal scanning of the focused laser beam in the back focal plane is required with our experimental setup since the illumination field is

uniform in TIRF. The working range is from zero degree (epi-illumination mode) to the maximum angle $\theta \approx 68$–$69°$ achievable with our oil immersion objective (Olympus PlanApoN 60x, NA = 1.45). Although the theoretical maximum angle given by the numerical aperture of the objective is about 72°, significant defects become more and more visible on TIRF pictures for $\theta > 69°$. A coherent laser source at 488 nm was used to excite the sample (Sapphire 488–200 mW, Coherent). The polarization of the incident laser beam was fixed in *s* configuration (TE). Then, the polarization state in TIRF is also in *s* configuration. Moreover, the illumination area of the sample is very large, allowing to observe simultaneously several cells (the lateral waist of the excitation profile is about 120 μm). In TIRF configuration, the laser beam is focused at the periphery of the pupil entrance of the objective and next propagates along the edge of the objective aperture. The fluorescence signal from the sample is collected by the same objective and imaged onto a CMOS camera (ORCA Flash 4.0, Hamamatsu). A fine achievement of the axial focusing is provided by a z-piezo device supporting the objective (Physik Instrumente, PI). Finally, the microscope is enclosed in an hermetic chamber to perform observations at 37 °C (Okolab enclosure).

2.2. Variable-angle TIRFM

Assuming that the plasma membrane of living cells is labeled with fluorescent molecules, the distance z_0 between the stained membrane and the substrate (Figure 1) can be measured with variable-angle total internal reflection fluorescence microscopy. vaTIRFM was described in detail in a previous publication [15]. Briefly, this technique involves the recording of a stack of several TIRF images, by gradually increasing the incident angle of the laser beam on the sample. 10 different TIRF images at 10 different incident angles are enough. The first angle is $\theta_1 = 63.6°$ and the last one is $\theta_{10} = 67.2°$, with an increment step of $\approx 0.4°$. The laser irradiance in epi-fluorescence, i.e., for $\theta = 0$, was fixed to 5 W/cm^2. To limit cell exposure, and so the photodamage of the specimen, each TIRF image was typically recorded in 25 or 100 ms. So, the total acquisition time for one vaTIRF run is typically in the range of $\approx$250 ms to $\approx$1 s (the rotational speed of the mirror is very fast, only a few milliseconds for each step of 0.4°). The leading approach is to take advantage of the dependence of the evanescent wave penetration depth on θ. This stack of images is then used to calculate pixel by pixel the water gap thickness z_0 between the membrane and the glass/water interface. Assuming that the detected fluorescence signal in TiRF is related to fluorescent molecules located on the ventral part of the cell, the fluorescence signal in each pixel (x, y) of the ith image of the series, denoted $f(x, y, \theta_i, z_0)$, can be used to calculate the membrane/substrate distance z_0 according to:

$$\ln \frac{f(x, y, \theta_i, z_0)}{\gamma(\theta_i)/\gamma(\theta_1)} = \Omega \; - z_0 \frac{4\pi}{\lambda_L} \sqrt{n_g^2 \sin^2(\theta_i) - n_{\text{eff}}^2} \tag{2.1}$$

$(\gamma(\theta_i)/\gamma(\theta_1))$ is the irradiance correction factor at the glass/water interface. For s-polarized light this factor is simply equal to $(\cos^2(\theta_i)/\cos^2(\theta_1))$. Ω includes all the unknown parameters which usually influence the contrast of TIRF images, such as the local concentration of dyes, their 3D orientation and the consequences on their absorption cross-section, angular emission pattern and radiative lifetime. λ_L is the laser wavelength. n_g and n_{eff} are respectively the glass refractive index and the effective refractive index of the sample. n_{eff} involves the presence of a cell in adhesion on the glass substrate. n_{eff} will increase together with the cytoplasmic refractive index. It also increases when the water gap thickness decrease. It is important to note that n_{eff} will be very high on specific adhesion zone, namely

on focal contacts, mainly due to the presence of various proteins such as actin cortex, focal adhesion kinase (FAK), vinculin, talin, etc. So, by plotting in each pixel the natural logarithm of the normalized fluorescence signal with respect to $\sin(\theta_i)$, Equation 1 can be used to fit the data in order to extract simultaneously z_0 and n_{eff}. Similar data processing can be done pixel by pixel, to obtain the cell surface topography (i.e. a map of the membrane/substrate distance z_0) and the n_{eff} cartography [15].

2.3. Sample preparation and cell culture

To investigate specific and nonspecific adhesion processes, glass coverslips were functionalized with two different biomolecules. Thickness-corrected glass coverslips were used as substrate (thickness 170 μm ± 10 μm, n_g = 1.5298 at λ_L = 488 nm and at room temperature, Assistant, Sondheim, Germany).

In order to observe specific adhesion, the glass surfaces were coated with a thin layer of fibronectin. The first step is to clean and activate the coverslips by immersion into freshly prepared piranha solution for at least 30 min (50% H_2O_2 and 50% H_2SO_4). The coverslips are then rinsed with ultra pure water and dried with argon gas. By doing so, the glass surfaces are negatively charged due to the presence of silanol groups (SiOH terminated). The second step is to incubate the cleaned coverslips in a solution of fibronectin (fibronectin from human plasma at 0.1%, Sigma-Aldrich, F0895) diluted in PBS at 10 μg/mL (phosphate buffer solution at pH = 7.2) during 1 hour. Fibronectin proteins are physisorbed as a result of electrostatic interactions between silanol (SiO^-) and their amine groups (NH_3^+). Finally, to remove the non-absorbed fibronectin on SiOH surfaces, coverslips were rinsed with ultra pure water and dried with argon gas. Nonspecific adhesion was observed on glass coverslips coated with poly-L-lysine. The coverslips were firstly cleaned by immersion in isopropanol and placed in an ultrasonic bath for 10 minutes. After that, they were dried with argon gas. Isopropanol cleaned coverslips were then incubated during 1 h with a poly-L-lysine solution diluted at 3% in PBS during 1 h (poly-L-lysine solution at 0.01%, MW = 150–300 kDa, Sigma-Aldrich, P4832). Finally, coverslips were washed with ultra pure water and dried with argon gas.

The coverslips coating were then characterized with contact angle measurement to ensure the homogeneity of the layer. Water contact angles were measured under ambient atmosphere at room temperature using the sessile drop method and an image analysis of the drop profile (OCA15EC system, Data Physics). As expected, SiOH surfaces are highly hydrophilic, with a contact angle < 6 degrees. After covering with fibronectin, the coverslips became hydrophobic, with a contact angle of 49 ± 2 degrees measured over several coverslips. On the contrary isopropanol cleaned coverslips are hydrophobic with a contact angle of 53 ± 2 degrees. The contact angle slightly increases to 66 ± 4 degrees after poly-L-lysine coating. The layer thickness in the air was estimated by ellipsometry on silicon wafer, according to the same surface functionalization (UVISEL, Horiba Jobin-Yvon). We obtained a mean layer thickness of 3 ± 2 nm and 4 ± 1 nm, respectively for poly-L-lysine and fibronectin.

MDA-MB-231 human breast cancer cells were grown in MEM medium (Minimum Essential Medium Glutamax-I, Gibco) supplemented with 10% of FBS (Fetal Bovine Serum, Gibco) and 1% of antibiotics (penicillin 100 U/mL and streptomycin 100 μg/mL, Gibco) in a humidified atmosphere at 37 °C with 5% CO_2. For vaTIRF observations, cells were placed in a chamber which contains a non-fluorescent culture medium at 488 nm. We used DMEM^{gfp}-2 medium (Dulbecco's Modified Eagle Medium, Evrogen), without phenol red, riboflavin and a low amount of folic acid. DMEM^{gfp}-2

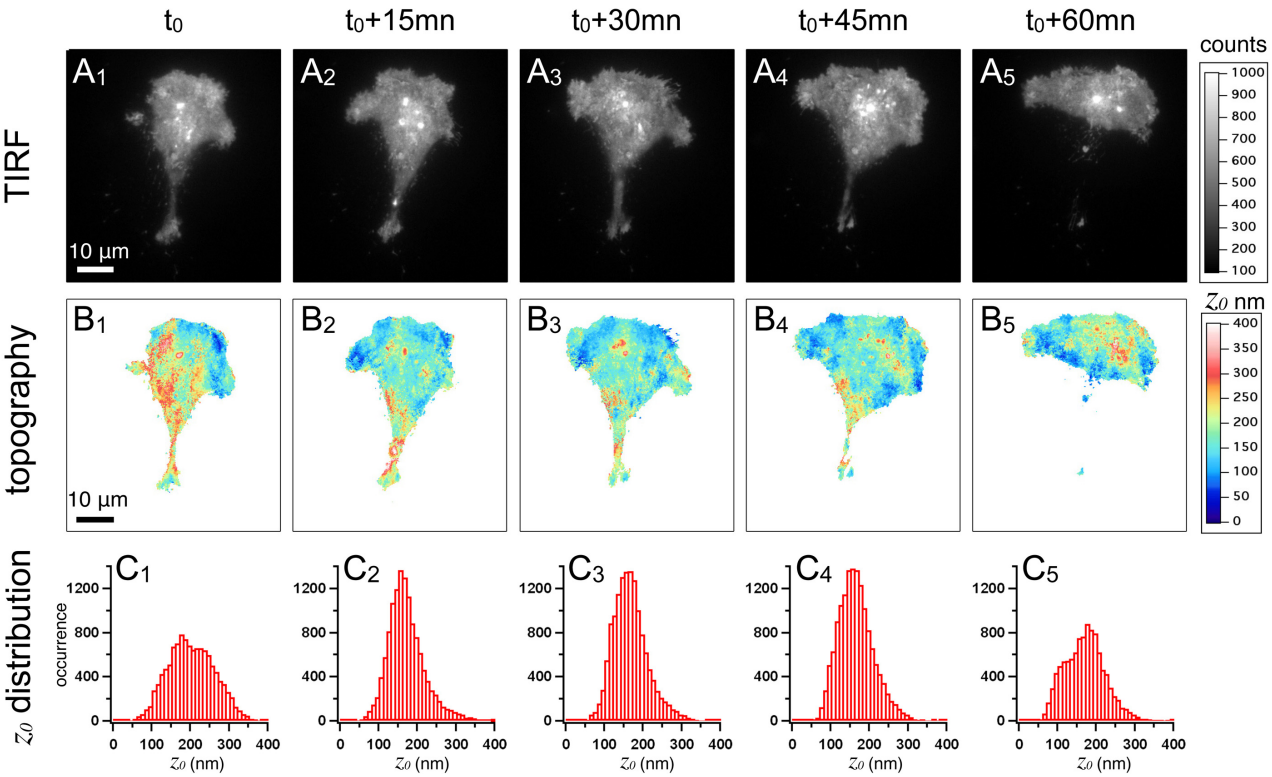

Figure 2. Typical example of adhesion dynamics of one MDA-MB-231 cell on fibronectin. (A_i): TIRFM images at different time for $\theta_1 = 63.6$ degrees. (B_i): the corresponding cell membrane topography and (C_i): the corresponding z_0-distance histogram.

was then supplemented with L-glutamine at 2 mM (Gibco), HEPES buffer at 10 mM (N-2-hydroxyethylpiperazine-N-2-ethane sulfonic acid, Gibco) and just 1% of FBS.

For plasma membrane labeling, we used well known DiO probe ($DiOC_{18}(3)$, 3,3'-Dioctadecyloxacarbocyanine Perchlorate, Molecular Probes D275). To stain the plasma membrane with DiO, $\sim 3 \times 10^5$ cells were suspended (using trypsin) in 1 mL of the non-fluorescent culture medium. Next, 7 μL of a solution of DiO diluted in DMF at 700 μM (previously sonicated) was gently mixed with cells and incubated for 10 minutes at 37 °C with 5% of CO_2 (the final concentration of DiO is about 5 μM). To remove the DiO molecules not internalized, labeled cells were washed three times by centrifugation at 1500 rpm for 5 minutes, by changing the non-fluorescent medium and resuspending the cells in warm medium between each spin. After the final spin, the MDA-MB-231 cells were placed into a homemade cylindrical hermetic chamber (to avoid evaporation) made with two coverslips and dedicated to optical observations. The lower coverslip was previously coated with fibronectin or poly-L-lysine. To promote the adhesion of cells, this sample was incubated for 1 hour at 37 °C in the presence of 5% of CO_2.

3. Results and Discussion

Several vaTIRFM acquisitions were done every 2 or 5 minutes on different MDA-MB-231 cells in adhesion on poly-L-lysine and on fibronectin. Two typical vaTIRFM measurements are presented in

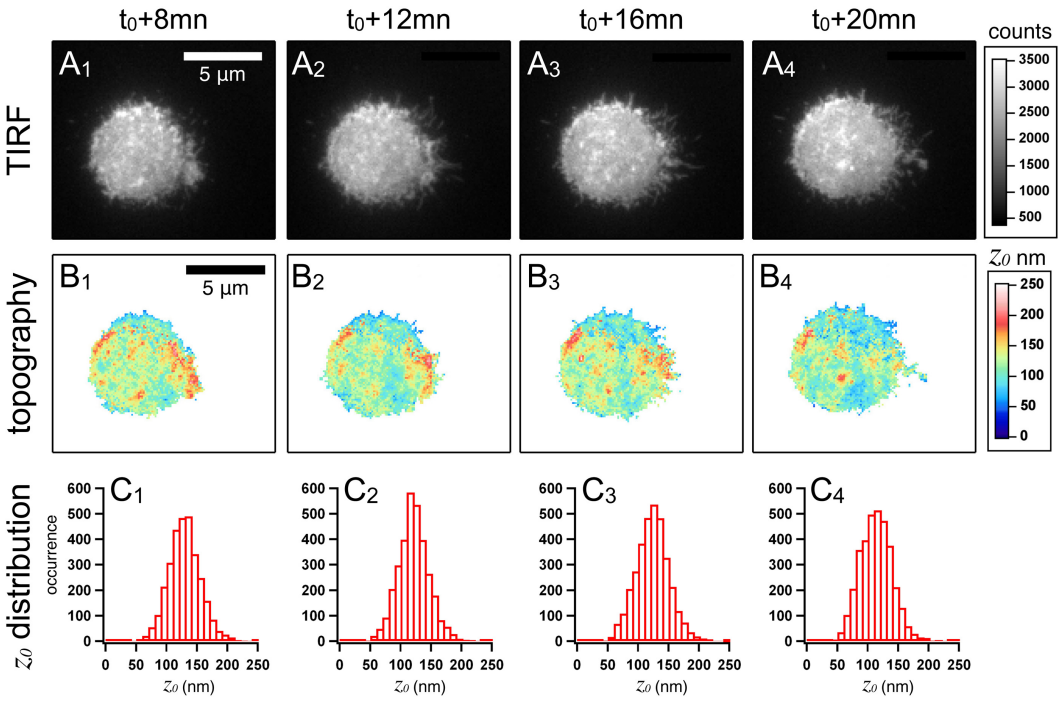

Figure 3. Example of adhesion dynamics of one MDA-MB-231 cell on poly-L-lysine. (A_i): TIRFM images at different time for $\theta_1 = 63.6$ degrees. (B_i): the corresponding cell membrane topography and (C_i): the corresponding z_0-distance histogram.

Figures 2 and 3. As expected, the presence of fibronectin on the surface enhance cell migration, as shown in Figure 2. Hence, one can recognize in Figures 2A_i the typical shape of motile cells, marked by a *teardrop* shape and more importantly, a large lamellipodium at the cell front. This example clearly indicates that the cell topography changes notably during the displacement. Furthermore, the dynamic of adhesion is quite fast. The close contacts located at the front of the cell (see the dark blue areas in Figures 2B_i) appear and disappear in only few minutes. The contours of z_0-distance distributions is also affected during the cell motion (Figures 2C_i). On the contrary, the behavior on poly-L-lysine is completely different. As shown in Figure 3, the cell contour is always circular. No migration was observed and the z_0-distance distributions recorded at different times are similar. These observations on fibronectin and poly-L-lysine are consistent with commonly accepted knowledges in cell biology: fibronectin surfaces promote the migration, whereas poly-L-lysine surfaces block the migration through a strong electrostatic attraction between the positively charged amine groups present at the glass surface and the negatively charged glycocalyx on the cell membrane.

As firstly proposed by D. Prieve. et al. in the end of 80 s for micro-sphere in interaction with flat surface [25, 26, 27], we will demonstrate that it is possible to extract from distributions of membrane/surface separation distances, the potential energy of cell membrane/substrate interactions (also known as the free energy of interactions). To our knowledge, such kind of analysis has never been realized on living cells, even though similar studies were realized with lipid membranes in adhesion on bare and functionalized glass coverslips [28, 29]. As explained in the introduction, the interactions between the cell and the surface are governed by specific and nonspecific forces. All the

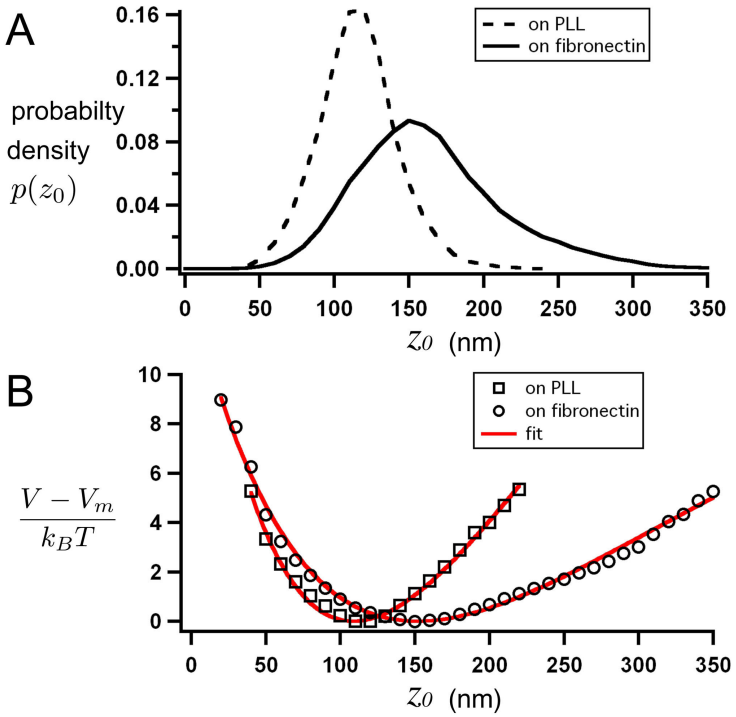

Figure 4. (A): Probability density $p(z_0)$ according to the vaTIRFM experiments presented in Figures 2 and 3. The distributions are plotted with a x-axis bin size of 10 nm. The number of vaTIRFM images used to reconstruct $p(z_0)$ is 12 for the cell on fibronectin and 11 for the cell on poly-L-lysine. (B): The corresponding potential energy $V(z_0)$ in k_BT unit. These data were fitted according to Equation 5. After the fitting procedure, we obtained $D_e = 28.7\ k_BT$ on poly-L-lysine and $D_e = 14.9\ k_BT$ on fibronectin.

molecules involved in these processes can freely move in accordance with the fluidity and elasticity of plasma membrane and also with the reorganization of the cytoskeleton. Therefore, *Brownian*-like motion of thermal origin will regulate the time-evolution of membrane/substrate separation distance z_0. Let us introduce $p(z_0)$ the probability density of finding the plasma membrane at a distance z_0 from the interface. Then, after a sufficient long time observation, the distribution $p(z_0)$ will be *Boltzmann* distributed:

$$p(z_0) = c_n e^{-V(z_0)/k_BT} \tag{3.1}$$

where c_n is a normalization factor chosen such that $\int p(z_0)dz_0 = 1$, k_BT the thermal energy and $V(z_0)$ the potential energy. The probability density $p(z_0)$ can be established through time lapse vaTIRFM measurements, as those presented in Figures 2 and 3. In practice, $p(z_0)$ was obtained by summing the z_0-distance histograms recorded at the different time lapses, and then by normalizing the resulting histogram in order to verify $\int p(z_0)dz_0 = 1$. By this way, one can acquire the typical distribution function $p(z_0)$ of a single cell (10–15 successive vaTIRFM acquisitions are enough). Two of these distributions are plotted in Figure 4A, regarding one cell in adhesion on poly-L-lysine and another on fibronectin. Hence by taking the negative logarithm of $p(z_0)$, Equation (2) gives:

$$\frac{V(z_0)}{k_BT} = -\ln p(z_0) + constant. \tag{3.2}$$

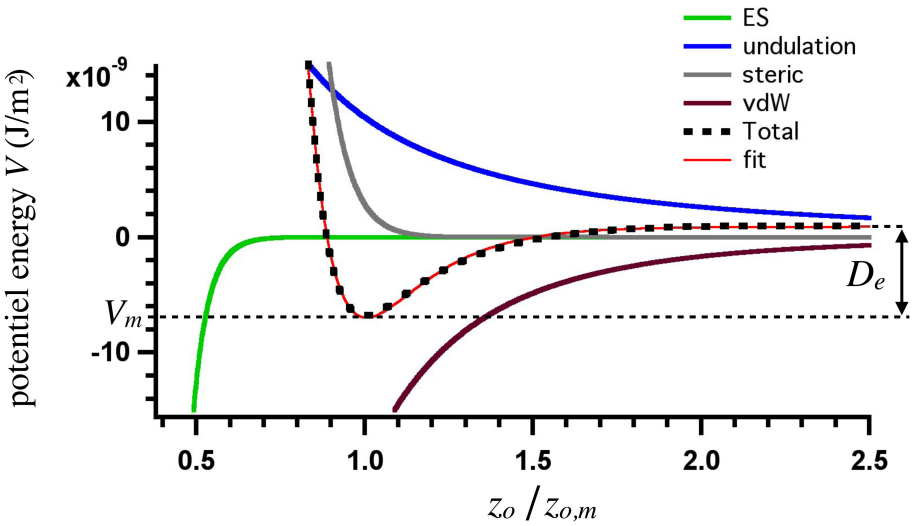

Figure 5. Total interaction potential (dashed line) between a lipid membrane and a glass substrate, calculated by superposition of van der Waals attraction (vdW), electrostatic attraction (ES), steric repulsion of glycocalyx and *Helfrich* undulation repulsion. For this calculation we consider a negatively charged lipid membrane (a lipid bilayer thickness of 5 nm, a surface potential of –20 mV, and a glycocalyx radius of gyration of 10 nm) in interaction with a positively charged fused silica substrate (a surface potential +25 mV), in water at 37 °C and with a Debye length of 1 nm. More details about this simulation is given in the Supporting Information. The total interaction potential was fitted according to Equation 5.

The constant in Equation (3) is given by the minimum value of $V(z_0)$. It depends on the normalization factor c_n, and so it changes with the bin size used to plot the distribution $p(z_0)$. Thus, one can get around this constant by plotting:

$$\frac{V(z_0) - V_m}{k_B T} = -\ln p(z_0) \tag{3.3}$$

where V_m is the minimum of $V(z_0)$. The corresponding membrane/surface separation distance is denoted $z_{0,m}$ ($V(z_{0,m}) = V_m$). By doing so, it is possible to obtain the profile of the global potential energy around its minimum, as shown in Figure 4B. Thereby, Equations (3) and (4) provide a direct method to determine the global potential of interaction. $V(z_0)$ includes the fingerprints of many interactions, both specific and nonspecific. Of course the ligand/receptor binding energy cannot be measured with our technique because we evaluate the distance from the substrate to the membrane and not the ligand/receptor interdistance. However, the interactions between ligands and receptors affect significantly the height of the membrane, which most closely approaches the substrate on focal adhesion zones, in a way that makes it possible to probe such specific events.

It appears clearly on Figure 4B that the profile of potential energy around its minimum is not symmetric and also not parabolic. This means that $V(z_0)$ cannot be approximated by a harmonic potential. One of the key features of the true $V(z_0)$ is that when the plasma membrane is at a great distance from the surface, the attractive force needs to be zero. Thus, $V(z_0)$ tends to a constant value when the cell is far away from the interface ($z_0 \to \infty$). This suggests that the model suited to depict

Table 1. Dissociation energy of MDA-MB-231 cells on poly-L-lysine and on fibronectin. $\langle D_e \rangle$ and σ_{D_e} are respectively the mean and the standard deviation between each cell of D_e. N is the number of cells studied on each surface.

	$\langle D_e \rangle$	σ_{D_e}	N
on fibronectin	16.2 k_BT	2.3 k_BT	8
on poly-L-lysine	29.1 k_BT	8.5 k_BT	8

membrane/substrate interactions is a anharmonic potential, as shown in reference [29]. Therefore, the best convenient mathematical expression that actually represents the potential energy of interactions has been proposed by Philip Morse in the context of vibrational energy of diatomic molecules [30, 31]:

$$V(z_0) = V_m + D_e \left(1 - e^{-\beta(z_0 - z_{0,m})}\right)^2 \tag{3.4}$$

where D_e is a dissociation energy and β a constant. D_e is the energy difference between the minimum of potential energy V_m and the asymptotic potential energy when $z_0 \to \infty$, as illustrated on Figure 5. To highlight the relevance of the *Morse* function in the context of cell membrane/substrate interactions, we have simulated the potential energy for a lipid bi-layer in interaction with a flat fused silica glass substrate (Figure 5). In this simulation we only consider nonspecific interactions (see Supporting Information). The lipid membrane is negatively charged and includes long polymer chains to emphasize the presence of glycocalyx at the cell surface. On the opposite side, the glass surface is positively charged to induce an electrostatic attraction. As shown in Figure 5, the simulated total interaction potential fits very well the *Morse* function (red curve). Thus, Equation (5) can be also used to fit the two experimental potential curves plotted in Figure 4B. Once again there is a good agreement between the data and the *Morse* function, meaning this model is relevant for membrane/substrate interactions. Hence, one can extract the values of D_e for these two cells. We have obtained $D_e = 28.7\ k_BT$ on poly-L-lysine and $D_e = 14.9\ k_BT$ on fibronectin. We carried out several vaTIRFM measurements on other cells. The results are given in Table 1. Likewise, the mean dissociation energy recorded on different single MDA-MB-231 cells on fibronectin is about twice smaller than on poly-L-lysine. This expected outcome highlights the strong interest for D_e to quantify the adhesion strength. The higher D_e, the higher cell is trapped onto the substrate, and its motility is thus inhibited. Therefore, it should be valuable to compare the adhesion strength, by measuring D_e, on different coatings (fibronectin, collagen IV, etc.) to study the role of focal adhesion contacts in cell signaling. In fact, it would be interesting to measure D_e for various integrin-based adhesion contacts as integrins constitute very attractive targets for inhibitors of anti-metastasis treatments. Such investigations are behind the scope of this paper, which is rather dedicated to highlight the feasibility of our technique. The dissociation energy measured in this paper (Table 1) is related to the plasma membrane composition and organization. Furthermore, D_e is an averaged value over the whole surface of contact between the cell membrane and the substrate. The values we have obtained have the same order of magnitude than ligand/receptor binding energy [32, 33, 34], but this is a coincidence without causal relationship.

Simulations on Figure 5 show that electrostatic interactions seem to have a small weight on the profile of potential energy $V(z_0)$. This is mainly due to the nanoscopic value of the *Debye* length

($\kappa^{-1} \lesssim 1$ nm) in any culture medium. However, our experimental results on poly-L-lysine clearly demonstrate that the electrostatic attraction is efficient enough to stick the cells to the substrate. In fact, the model used to calculate electrostatic interactions in Figure 5 (see Supporting Information) considers two different parallel and flat charged surfaces (the charges are found on the interfaces). In our experimental case, the poly-L-lysine on the glass substrate and the glycocalyx on the cell enveloppe constitute two layers with thicknesses from few nanometers to few tens of nanometers. Furthermore, the charges within these two layers are randomly located along the polymer chain for poly-L-lysine and along the branched chains of oligosaccharides for glycocalyx. To add further complexity, all these charges can diffuse according to various processes. To our knowledge, there is no generic model in the literature to depict this complex interaction, and this constitutes a crucial issue to understand cell/substrate interactions.

4. Conclusion

We proposed in this paper a new method, to our knowledge, to quantify adhesion strength at the single cell level. By observing the plasma membrane over all the contact area with the substrate, vaTIRFM was used to reconstruct the cell membrane topography with a nanometric axial resolution. From the time-evolution of the topography, one can extract the profile of potential energy related to cell membrane/substrate interactions. This profile can be fitted with the *Morse* function in order to obtain the dissociation energy D_e connected to the adhesion strength. In the case of MDA-MB-231 cells in adhesion on poly-L-lysine and fibronectin, we have shown that D_e is a relevant parameter to precisely quantify the adhesion. These results open new promising perspectives in the context of integrin-mediated migration processes. In addition to its key role as signaling center, integrins can also transmit contractile forces that arise from cytoskeleton tension. Thus, it would be also very interesting to combine vaTIRFM with another optical tool to observe cytoskeleton forces as traction force microscopy (TFM). This requires to coat the coverslip with an elastic gel doped with fluorescent nanobeads. But, to properly realize TIRF microscopy the refractive index of the gel must match the refractive index of the coverslip that is ≈ 1.53 at 488 nm. Silicone gels commonly used in TFM such as polyacrylamide or PDMS (polydimethylsyloxane) are not suitable for TIRF. Interesting work by E. Gutierrez. et al. recently proposed to use a high refractive index silicone gels to achieve simultaneously TIRF microscopy and TFM [35].

Acknowledgments

The authors thank Christophe Couteau for his careful reading of this article. This work was supported by the Conseil Régional Champagne-Ardenne, the Fond Européen de Développement Régional: CELLnanoFLUO project, the ligue Contre le Cancer (Comité de l'Aube), le Grand Troyes and the Conseil Départemental de l'Aube.

Conflict of Interest

The authors declare no conflict of interests in this paper.

References

1. Roca-Cusachs P, Gauthier NC, del Rio A, et al. (2009) Clustering of $\alpha_5\beta_1$ integrins determines adhesion strength whereas $\alpha_v\beta_3$ and talin enable mechanotransduction. *PNAS* 106: 16245–16250.
2. Hynes RO (2002) Integrins: bidirectional, allosteric signaling machines. *Cell* 110: 673–687.
3. Geiger B, Spatz JP, Bershadsky AD (2009) Environmental sensing through focal adhesion. *Nat Rev Mol Cell Biol* 10: 21–33.
4. Sackmann E, Bruinsma RF (2002) Cell adhesion as wetting transition? *Chem Phys Chem* 3: 262–269.
5. Limozin L, Sengupta K (2007) Modulation of vesicle adhesion and spreading kinetics by hyaluronan cushion. *Biophys J* 93: 3300–3313.
6. Sackmann E, Smith AS (2014) Physics of cell adhesion: some lessons from cell-mimetic systems. *Soft Matter* 10: 1644–1659.
7. Paszek MJ, DuFort CC, Rossier O, et al. (2014) The cancer glycocalyx mechanically primes integrin-mediated growth and survival. *Nature* 511: 319–325.
8. Feghhi S, Munday AD, Tooley WW, et al. (2016) Glycoprotein Ib-IX-V complex transmits cytoskeletal forces that enhance platelet adhesion. *Biophys J* 111: 601–608.
9. Labouesse C, Verkhovsky AB, Meister JJ, et al. (2015) Cell shape dynamics reveal balance of elasticity and contractility in peripheral arcs. *Biophys J* 108: 2437–2447.
10. Rupprecht P, Gol L, Rieu JP, et al. (2012) A tapered channel microfluidic device for comprehensive cell adhesion analysis, using measurements of detachment kinetics and shear stress-dependent motion. *Biomicrofluidics* 6: 014107.
11. Visser CW, Gielen MV, Hao Z, et al. (2015) Quantifying cell adhesion through impingement of a controlled microjet. *Biophys J* 108: 23–31.
12. Sariisik E, Popov C, Mller JP et al. (2015) Decoding cytoskeleton-anchored and non-anchored receptors from single-cell adhesion force data. *Biophys J* 109: 1330–1333.
13. Partridge MA, Marcantonio EE (2006) Initiation of attachement and generation of mature focal adhesions by integrin-containing filopodia in cell spreading. *Mol Biol Cell* 17: 4237–4248.
14. Kanchanawong P, Shtengel G, Pasapera AM, et al. (2010) Nanoscale architecture of integrin-based cell adhesion. *Nature* 468: 713–724.
15. Dos Santos MC, Déturche R, Vézy C, et al. (2016) Topography of cells revealed by variable-angle total internal reflection fluorescence microscopy. *Biophys J* 111: 1316–1327.
16. Limozin L, Sengupta K (2009) Quantitative reflection interference contrast microscopy (RICM) in soft matter and cell adhesion. *Chem Phys Chem* 10: 2752–2768.
17. Paszek MJ, DuFort CC, Rubashkin MG, et al. (2012) Scanning angle interference microscopy reveals cell dynamics at the nanoscale. *Nat Methods* 9: 825–827.
18. Chizhik AI, Rother J, Gregor I, et al. (2014) Metal-induced energy transfer for live cell nanoscopy. *Nat Photonics* 8: 124–127.
19. Bourg N, Mayet C, Dupuis G, et al. (2015) Direct optical nanoscopy with axially localized detection. *Nat Photonics* 9: 587–593.

20. Waldchen S, Lehmann J, Klein T, et al. (2015) Light-induced cell damage in live-cell super-resolution microscopy. *Sci Rep* 5: 15348.

21. Johansson S, Svineng G, Wennerberg K, et al. (1997) Fibronectin-integrin interactions. *Front Biosci* 2: d126–d146.

22. Bartsch JE, Staren ED, Appert HE (2003) Adhesion and migration of extracellular matrix-stimulated breast cancer. *J Surg Res* 110: 287–294.

23. Wong NC, Mueller BM, Barbas CF, et al. (1998) α_v Integrins mediate adhesion and migration of breast carcinoma cell lines. *Clin Exp Metastasis* 16: 50–61.

24. Mierke CT, Frey B, Fellner M, et al. (2010) Integrin $\alpha_5\beta_1$ facilitates cancer cell invasion through enhanced contractile forces. *J Cell Sci* 124: 369–383.

25. Prieve DC, Alexander BM (1986) Hydrodynamic measurement of double-layer repulsion between colloidal particle and flat plate. *Science* 231: 1269–1270.

26. Prieve DC, Bike SG, Frej NA (1990) Brownian motion of a single microscopic sphere in a colloidal force field. *Faraday Discuss Chem Soc* 90: 209–222.

27. Prieve DC, Frej NA (1990) Total internal reflection microscopy: a quantitative tool for the measurement of colloidal forces. *Langmuir* 6: 396–403.

28. Radler J, Sackmann E (1992) One the measurement of weak repulsive and frictional colloidal forces by reflection interference contrast microscopy. *Langmuir* 8: 848–853.

29. Schmidt D, Monzel C, Bihr T, et al. (2014) Signature of nonharmonic potential as revealed from a consistent shape and fluctuation analysis of adherent membrane. *Phys Rev X* 4: 021023.

30. Morse PM (1929) Diatomic molecules according to the wave mechanics. II Vibrational levels. *Phys Rev* 34: 57–64.

31. Herzberg G (1950) *Molecular spectra and molecular structure. I. Spectra of diatomic molecules*, 2 Eds., New York: D. Van Nostrand Company, INC.

32. Merkel R, Nassoy P, Leung A, et al. (1999) Energy landscapes of receptor-ligand bonds explored with dynamic force spectroscopy. *Nature* 397: 50–53.

33. Li F, Redick SD, Erickson HP, et al. (2003) Force measurements of the $\alpha_5\beta_1$ integrin-fibronectin interaction. *Biophys J* 84: 1252–1262.

34. Robert P, Nicolas A, Aranda-Espinoza S, et al. (2011) Minimal encounter time and separation determine ligand-receptor binding in cell adhesion. *Biopjys J* 100: 2642–2651.

35. Gutierrez E, Tkachenko E, Besser A, et al. (2011) High refractive index silicone gels for simultaneous total internal reflection fluorescence and traction force microscopy of adherent cells. *PloS One* 6: e23807.

AIMS Press